This document is a preprint of: F. Roth, N. Bidoul, T. Rosca, *et al.*, "Spike-based sensing and communication for highly energy-efficient sensor edge nodes," in *Proc. 2nd IEEE Int. Hybrid Symp. Joint Communications & Sensing (JC&S)*, Accepted for publication, Innsbruck, Austria, Mar. 2022.

Spike-Based Sensing and Communication for Highly Energy-Efficient Sensor Edge Nodes

Florian Roth*, Noémie Bidoul‡, Teodor Rosca†, Meik Dörpinghaus*,
Denis Flandre‡, Adrian M. Ionescu†, and Gerhard Fettweis*
*Vodafone Chair Mobile Communications Systems, Technische Universität Dresden, 01062 Dresden, Germany
{florian.roth2, meik.doerpinghaus, gerhard.fettweis}@tu-dresden.de
‡Institute of Information and Communication Technologies (ICTEAM), UCLouvain, Louvain-la-Neuve, Belgium
{noemie.bidoul, denis.flandre}@uclouvain.be
†Nanoelectronic Devices Laboratory (NANOLAB) - EPFL, Lausanne, Switzerland
{teodor.rosca, adrian.ionescu}@epfl.ch

***Abstract*—Highly energy-efficient wireless sensor nodes are a prerequisite for a sustainable operation of the Internet of things. Therefore, classical approaches for system design based on digital signal processing are not a viable solution, but system design has to follow entirely new paradigms. In this regard, we present a sensory system with analog spike-based signal processing for sensing and communication, encoding the sensory information in the pulse repetition frequency (PRF), getting rid of energy hungry A/D and D/A conversion. Our spiking sensory system can generate spikes from any conventional analog output sensor using a compact, highly tunable voltage-controlled oscillator based on vanadium dioxide, and an analog differentiator circuit performing the transmit pulse shaping. The sole conversion from analog to digital takes place at the base station followed by the estimation of the PRF, for which we compare a conventional receiver design consisting of an analog-to-digital converter (ADC) with the use of an integrate-and-fire time encoding machine (IF-TEM). Results show the successful communication of sensory information from the edge node over an additive white Gaussian noise channel to the base station, with the IF-TEM outperforming the conventional ADC for a signal-to-noise ratio above 0 dB.**

***Index Terms*—spike-based signaling, analog processing, metal-to-insulator transition, A/D conversion, frequency estimation**

I. Introduction

Sensory data plays a key role for present and future services and applications. It is expected that the number of battery-powered mobile sensor edge nodes in the Internet of things (IoT) will increase drastically calling for highly energy-efficient sensing, processing, and wireless transmission [1]. Up to date the energy consumption of these steps is not compatible with a sustainable operation of the IoT as shown in [2], nor with high battery lifetime requirements crucial in many application fields [3]. To reduce the energy consumption, new designs of information processing systems get inspiration from biological systems, as so far no technical solution has reached the energy efficiency of the human nervous system [4]. It encodes information in the time domain instead of the amplitude using spike trains for sensing, processing, and transmission [5]. The first spiking sensors adopting this signal representation have been designed for visible light and pressure stimuli in [6] and [7], respectively. Highly energy-efficient processing is possible with spiking neural networks as presented in [8] while spike-like wireless communications can achieve an ultra low energy consumption of $24\,\mathrm{pJ/bit}$ as shown for impulse-radio ultra-wideband (IR-UWB) in [9] given relaxed requirements for the spectral efficiency [10]. In [9] and [11], variations of binary pulse position modulation are used together with simple energy detection at the receiver, hence limiting the amount of information which can be encoded in one pulse. Another way of encoding information in the time domain is the use of run-length limited (RLL) sequences as they are used in zero-crossing modulation (ZXM) to save energy at the receiver by using 1-bit analog-to-digital converters (ADCs) [12], [13] and in the spike-based time-derived zero-crossing modulation (TD-ZXM) to additionally save energy at the transmitter [10]. When attempting to design an energy-efficient processing chain, most works focus on the optimization of sensing, processing, and transmission individually. Due to the available compute power and reliability of CMOS technology, digital signal processing (DSP) is nowadays the standard throughout the processing chain starting with sensor signal processing up to digital modulation. While this approach allows for a modular design, it requires the conversion of the signal from analog to digital and vice versa. As the conversions, here from measured physical quantities to digital signals and from digital modulation to analog RF signals, cost energy, the motivation is to stay in the analog spike domain, in which the sensor information is provided.

Previous work in this direction includes [14], where analog circuitry is used to preprocess and classify the sensor signal without the use of ADCs. An event detection logic generates a wake-up signal activating a digital circuit for further processing or communication. Additionally, [15] proposes a *dumb-sensing and smart-processing* architecture where the all-analog sensor node performs only sensing while all the processing happens after wireless transmission in the digital domain at less denser distributed nodes of the network.

In this work, we propose a processing chain operating in the analog spike domain covering the sensor and the wireless

This work has been supported in part by the German Federal Ministry of Education and Research (BMBF) (6G-life, project-ID 16KISK001K). Computations were performed at the Center for Information Services and High Performance Computing (ZIH) at TU Dresden.

978-1-6654-0579-9/22/$31.00 ©2022 IEEE

This document is a preprint of: F. Roth, N. Bidoul, T. Rosca, *et al.*, "Spike-based sensing and communication for highly energy-efficient sensor edge nodes," in *Proc. 2nd IEEE Int. Hybrid Symp. Joint Communications & Sensing (JC&S)*, Accepted for publication, Innsbruck, Austria, Mar. 2022.

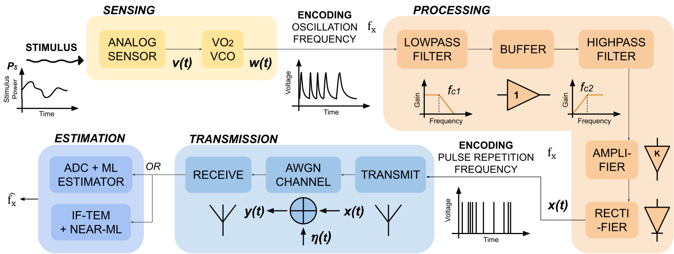

Fig. 1. Block scheme of the all-spiking analog processing chain

transmission to the base station. Only there the conversion into the digital domain is performed to allow for further processing. We avoid extensive sensor signal processing but keep the information encoded in the pulse repetition frequency (PRF) as it is provided by the spiking sensor. As the emitted spike train is of high bandwidth and the use of IR-UWB signals is suitable for radar applications as demonstrated in, e.g., [16], it is envisioned to extend the functionality of the presented sensor node by detecting backscatter to perform distance ranging - thus using the same signal for communication to the base station and for radar sensing.

This paper is organized as follows: In Section II the system model of the overall signaling chain is described. The design of the spiking sensor and the transmitted waveform are presented in Section III while Section IV covers the A/D conversion and estimation of the information-carrying PRF at the receiver. Simulation results on the system performance are given in Section V followed by concluding remarks in Section VI.

II. System Model

The block scheme of the proposed processing chain is given in Fig. 1. Here, we give a short description of the overall system, whereas the individual blocks are detailed in the subsequent sections. The first block of our wireless sensory system can be any sensor measuring a physical quantity, such as for example the power of incident light of the visible spectrum. The analog voltage output of the sensor $v(t)$ is then fed to an ultra compact, highly tunable voltage-controlled oscillator (VCO) based on vanadium dioxide. The latter encodes the sensory information into the frequency f_x of the VCO output oscillations. This signal $w(t)$ is further processed by simple analog circuitry converting it into a spike train, i.e., pulses of equal short duration with information encoded in the PRF f_x. The resulting wideband spike train $x(t)$ is then directly transmitted over an additive white Gaussian noise (AWGN) channel, adding the noise $\eta(t)$ with power spectral density (PSD) $N_0/2$, without any conversion into the digital domain that today's digital modulation techniques would require. To extract the sensory information from the received signal $y(t)$, the sole estimation of the PRF f_x is sufficient, giving its known dependency on the physical quantity to be measured. As the latter is assumed to vary slowly compared to the PRF f_x, the sensor node does not need to transmit the output of the oscillator permanently but transmits only K consecutive pulses at once to save energy. During these K spikes the PRF f_x is therefore assumed to be constant. This raises the question whether there is an optimal

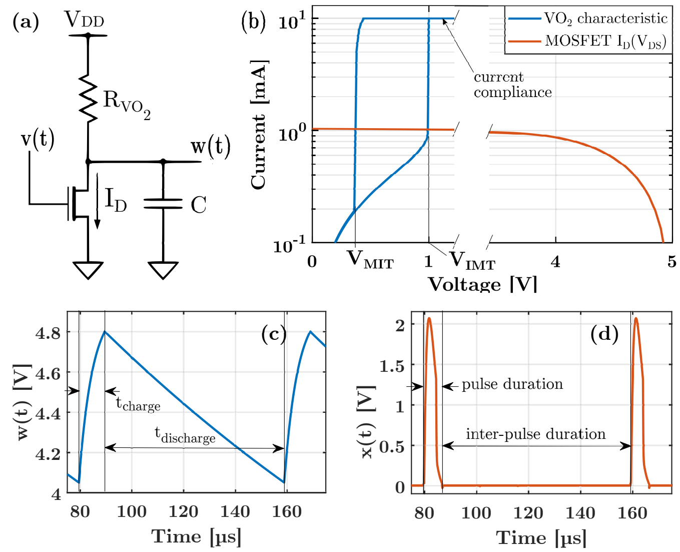

Fig. 2. (a) Schematics of the voltage-controlled oscillator, composed of the VO_2 resistive device, a MOSFET and an output capacitance, (b) Measurement of the current voltage characteristic of a typical VO_2 resistive device, along with the MOSFET characteristic, (c) Typical oscillation at the output of the sensing block for I_D = 2 mA, yielding f_x = 12.5 kHz, (d) The same waveform after the analog processing block, now consisting of short spikes.

choice of K, i.e., whether it is advantageous to transmit fewer pulses of higher amplitude, or more pulses of lower amplitude.

III. Sensor Design and Waveform

As stated above, the versatile sensing block can be composed of any conventional sensor with an analog voltage output, interfaced with a VCO leveraging the physical properties of a phase change material (vanadium dioxide - VO_2) to generate highly tunable, frequency-encoded oscillations. The oscillator, shown in Fig. 2 a), consists of a simple RC circuit loaded with an n-type MOSFET. The resistive element is a micrometer scale two-terminal VO_2 device which exhibits reversible Insulator-to-Metal phase transitions when voltages exceeding certain thresholds are applied across its terminals [17]. It can hence be used as a voltage-controlled resistance with two possible resistive states $R_{\mathrm{VO_2,met}}$ and $R_{\mathrm{VO_2,ins}}$, as visible in its hysteretic I-V curve in Fig. 2 b). The Metal-to-Insulator and Insulator-to-Metal transition voltages are referred to as respectively V_MIT and V_IMT. The DC operating point of the circuit is set by the intersections of the MOSFET output characteristic and the VO_2 I-V curve: When these intersections correspond to the transition regions of the VO_2 device, the circuit enters an astable configuration and the VO_2 device subsequently alternates between its metallic and insulating state, resulting in oscillations of the output voltage. A dynamic analytical model of the oscillator has previously been detailed and experimentally validated in [18], and shows that the charge and discharge durations within an oscillation period depend on the MOSFET drain current I_D (see equations (1) and (2)). The oscillation frequency can thus be made dependent on analog sensor readings by feeding the sensor voltage output $v(t)$ to the VO_2 oscillator MOSFET gate connection, as shown in Fig. 2 a). As demonstrated in [18], the oscillator displays a high tuning

This document is a preprint of: F. Roth, N. Bidoul, T. Rosca, *et al.*, "Spike-based sensing and communication for highly energy-efficient sensor edge nodes," in *Proc. 2nd IEEE Int. Hybrid Symp. Joint Communications & Sensing (JC&S)*, Accepted for publication, Innsbruck, Austria, Mar. 2022.

range exceeding 400% from 5 to 25 kHz, when the MOSFET gate voltage is varied from 2.5 to 5 V.

$$t_{\text{charge}}(I_\text{D}) = -R_{\text{VO}_2,\text{met}}\, C \cdot \ln \frac{V_\text{MIT} - R_{\text{VO}_2,\text{met}} I_\text{D}}{V_\text{IMT} - R_{\text{VO}_2,\text{met}} I_\text{D}} \quad (1)$$

$$t_{\text{discharge}}(I_\text{D}) = -R_{\text{VO}_2,\text{ins}}\, C \cdot \ln \frac{V_\text{IMT} - R_{\text{VO}_2,\text{ins}} I_\text{D}}{V_\text{MIT} - R_{\text{VO}_2,\text{ins}} I_\text{D}} \quad (2)$$

The dynamic model from [18] is used here to generate the oscillation waveforms for various drain currents, hence oscillator frequencies, ranging from $f_\text{min} = 5\,\text{kHz}$ to $f_\text{max} = 23\,\text{kHz}$. An example of such waveform is shown in Fig. 2 c), for $f_\text{x} = 12.5\,\text{kHz}$. These modeled waveforms are then used in subsequent simulations throughout the whole signaling chain. For the sake of energy-efficient communication, requiring good estimation of the frequency f_x to retrieve the associated stimulus power, and possible distance ranging using the emitted signal, the raw sawtooth oscillations generated by the oscillator are not the best choice. Instead, spike trains consisting of short, constant duration pulses would be desirable, with information encoded into the PRF rather than the oscillation period. To achieve such conversion, we present the following analog processing chain: it leverages the fact that during the charging cycle of the VCO, the charging current is governed by the metallic state resistance of the VO_2 element $R_{\text{VO}_2,\text{met}}$, rather than the MOSFET drain current, which has low authority over the circuit dynamics, making the time duration of the charging cycle quasi-independent of sensor bias. The different elements of the analog processing chain are summed up in Fig. 1: first, a buffered low-pass filter (LPF) filters out the high frequency noise. It is then followed by a high-pass filter (HPF) whose time constant is chosen such that the frequency of oscillation is outside its pass band. This enables the HPF to work as a derivator circuit that enhances fast changes in its input signal. The derivator circuit enables extraction of the rise time of the VCO, while the rectifier circuit that follows eliminates unwanted negative voltages corresponding to the VCO fall time. The resulting waveform, simulated through SPICE starting from the modeled oscillator output, is visible in Fig. 2 d). As shown in Fig. 3 (in log-scale), the variation of pulse duration w.r.t. the total period variation is negligible (although slightly increasing for higher frequencies). Therefore, for further processing, a single spike in $x(t)$ is assumed to have the pulse shape $g(t)$ of constant duration T_g, and a 95% power containment bandwidth B_g. In conclusion, the proposed analog processing chain enables conversion from a sawtooth waveform (where information is frequency-encoded) to a pulse train with minimally varying pulse widths, where information is encoded in its PRF.

IV. A/D Conversion of the Spike Rate

To retrieve the sensor information at the base station the PRF f_x must be estimated. We will compare two approaches that use different hardware to yield different digital representations of the received analog signal

$$y(t) = \frac{1}{\sqrt{K}} \sum_{k=0}^{K-1} a_k(f_\text{x})\, g\left(t - \frac{k}{f_\text{x}} - \Delta t\right) + \eta(t), \quad (3)$$

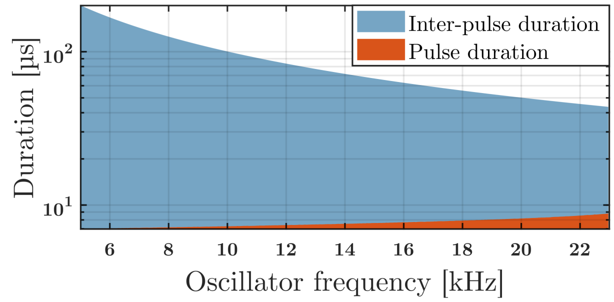

Fig. 3. Variation of pulse and inter-pulse duration with oscillator frequency, after the pulse shaping performed by the analog processing circuitry

where the amplitude $a_k(f_\text{x}) \approx 1$ is not a constant but varies due to the analog filtering and Δt is caused by lack of time synchronization. The scaling by $1/\sqrt{K}$ keeps the transmit energy independent of the number of pulses K.

A. ML-Estimation for Conventional A/D Conversion

First we consider the classical receiver architecture at the base station consisting of an ideal lowpass with cutoff frequency $f_\text{c} \geq B_\text{g}$ followed by a high resolution ADC sampling at Nyquist rate $T = 1/(2f_\text{c})$ giving the samples y_n. Neglecting the amplitude variation and timing offset, deriving the maximum likelihood (ML) estimate for the PRF yields

$$\hat{f}_{\text{x,ML}} = \underset{\check{f}_\text{x}}{\text{argmax}} \sum_{k=0}^{K-1} z\left(\frac{k}{\check{f}_\text{x}} + T_\text{g}\right). \quad (4)$$

In this expression $z(t)$ is the output of the matched filter $g_\text{MF}(t) = g(T_\text{g} - t)$ given by

$$z(t) = \sum_{n=-\infty}^{\infty} y_n\, g_\text{MF}(t - nT) \quad (5)$$
$$= (y * g_\text{MF})(t). \quad (6)$$

Eq. (6) holds due to the Shannon-Nyquist sampling theorem fulfilled for both $y(t)$ and $g_\text{MF}(t)$. Therefore, the matched filter can be applied in analog or digital and (4) can be evaluated by sampling and adding up the matched filter output $z(t)$ at different rates $\check{f}_\text{x}$. To get a sufficiently high resolution of f_x one has to test for a large number of PRFs $\check{f}_\text{x}$ requiring various ADCs operating at different rates. This would increase the hardware requirements drastically thus making this approach unfeasible. However, the evaluation of (4) is also possible in the frequency domain only performing simple matrix operations. For the derivation we add the term $nT, n = 0, 1, \ldots, N-1$ in the argument of $z(t)$ but evaluate the expression only at $n = 0$:

$$\hat{f}_{\text{x,ML}} = \underset{\check{f}_\text{x}}{\text{argmax}} \left\{ \sum_{k=0}^{K-1} z\left(nT + \frac{k}{\check{f}_\text{x}} + T_\text{g}\right)\Bigg|_{n=0} \right\} \quad (7)$$

$$= \underset{\check{f}_\text{x}}{\text{argmax}}\, \text{IDFT}\left\{ \text{DFT}\left\{ \sum_{k=0}^{K-1} z\left(nT + \frac{k}{\check{f}_\text{x}} + T_\text{g}\right)\right\}\right\}\Bigg|_{n=0} \quad (8)$$

$$= \underset{\check{f}_\text{x}}{\text{argmax}} \sum_{m=0}^{N-1} Z[m] \sum_{k=0}^{K-1} e^{j2\pi \frac{m}{NT}\left(\frac{k}{\check{f}_\text{x}} + T_\text{g}\right)}. \quad (9)$$

with $Z[m]$ being the discrete Fourier transform (DFT) of $z[n] = z(nT)$. Moreover, IDFT denotes the inverse DFT. Still, only a finite number of PRFs $\check{f}_{\mathrm{x},l}, l = 0, 1, \ldots, L-1$ can be evaluated. For a sufficiently high value of L, (9) can be simplified to

$$\hat{f}_{\mathrm{x,ML}} \approx \check{f}_{\mathrm{x},\hat{l}}, \quad \hat{l} = \underset{l}{\operatorname{argmax}}\ [\mathbf{C}\,\mathbf{D}\,\mathbf{z}]_l, \tag{10}$$

where $\mathbf{z} = [z[0]\ z[1]\ \ldots\ z[N-1]]^{\mathrm{T}} \in \mathbb{R}^{N\times 1}$ contains the samples of the matched filter output taken at Nyquist rate T, $\mathbf{D} \in \mathbb{C}^{N\times N}$ is the DFT matrix, $[\cdot]_l$ is the l-th entry of the argument vector, and the elements of $\mathbf{C} \in \mathbb{C}^{L\times N}$ are given by

$$[\mathbf{C}]_{l,m} = \sum_{k=0}^{K-1} e^{j2\pi \frac{m}{NT}\left(\frac{k}{\check{f}_{\mathrm{x},l}} + T_{\mathrm{g}}\right)}. \tag{11}$$

A signal repeated in time at frequency f_{x} has a spectrum in which peaks are placed f_{x} apart. Hence, (10) can be understood as searching for the series of peaks in the frequency domain for which the distance between peaks best matches the distance between peaks in the spectrum of $z(t)$. As $\mathbf{D}$ and $\mathbf{C}$ do not depend on the received data, they can be precomputed allowing for an efficient matrix-vector multiplication at runtime based on a standard receiver design using a fixed sampling rate as shown in Fig. 4 a). In addition, studying this receiver architecture and the succeeding PRF estimation in the digital domain in (10), it stands out that the pulse shape only has an impact on the matched filter but not on the DSP. Therefore, (10) is suitable to estimate the PRF from samples of any finite periodic spike-train with maximized SNR and stationary colored noise.

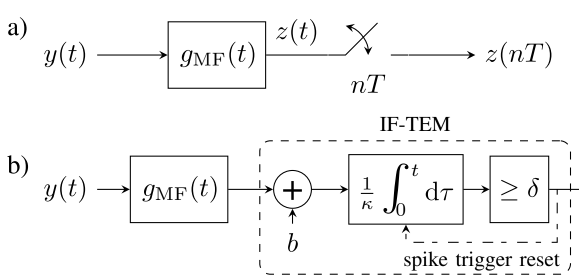

Fig. 4. The two receiver architectures used for digitization. In a) a conventional sampling generates evenly spaced samples while the IF-TEM in b) makes use of an integrator and a comparator resulting in the irregularly spaced discrete time instances t_n. An analog matched filter is used in both designs.

B. Integrate-and-Fire Time Encoding Machine

Given the received signal from (3), there are multiple reasons not to use the conventional receiver design shown in Fig. 4 a), but to use other methods that allow the acquisition and digitization of the PRF f_{x}. First of all, when the information is encoded solely in the time domain, it is counterintuitive to take high resolution values in the amplitude domain at evenly spaced time-instances if only information in the time domain is relevant. Is it not possible to take the encoding in the time domain into account when retrieving digital samples in the first place? Secondly, as we consider spikes which are narrow in time domain, eventually having a bandwidth of multiple GHz, the required sampling rates increase just as well leading to a rising power consumption of conventional ADCs [19]. Both of these caveats are considered when using an integrate-and-fire time encoding machine (IF-TEM) instead, the design of which is shown in Fig. 4 b), see, e.g., [20]. In [21] it was shown that IF-TEMs allow for perfect reconstruction of bandlimited signals and in [20] an IF-TEM is used to retrieve pulse positions in non-bandlimited periodic signals with known pulse shape and period and therefore limited number of degrees of freedom. The recovery method presented in [20] also works in the presence of noise.

To maximize the SNR at the input of the IF-TEM in this work a matched filter is used just as in the conventional receiver architecture, giving the time continuous signal $z(t) = (y * g_{\mathrm{MF}})(t)$. For perfect recovery the input of the IF-TEM must be bounded by some constant, i.e., $|z(t)| < c < b$. In this case, adding the bias b makes the resulting signal greater than zero, which is then scaled by $1/\kappa$ and integrated. When the output of the integrator exceeds the threshold δ, the current time instant $t_n, n = 1, 2, \ldots, M$ is output, having the time resolution of the local clock. Moreover, exceeding the threshold resets the output of the integrator to zero. Therefore, the relation between the input and output of the IF-TEM is described by

$$\kappa\delta = \int_{t_{n-1}}^{t_n} (z(t) + b)\,\mathrm{d}t. \tag{12}$$

As the transmitted signal $x(t)$ consists only of positive pulses, the reason for adding the bias b is not obvious, but it makes a negative output of the integrator unlikely. Otherwise when integrating a negative noise signal, the following spike might not exceed the threshold allowing the noise variance to increase even further. In the noiseless case when $z(t) \in [0, c]$ the firing rate $F_{\mathrm{R}} = (t_n - t_{n-1})^{-1}$ is bounded by

$$\frac{b}{\kappa\delta} \leq F_{\mathrm{R}} \leq \frac{b+c}{\kappa\delta}. \tag{13}$$

Given a non-negative integrator input, we want to be able to bound the average firing rate $\overline{F}_{\mathrm{R}}$ by some value $\overline{F}_{\mathrm{R}}^{*}$. With the simplifying assumption that the firing rate will reach its maximum for the entire duration of the spike after the matched filter, which is $2T_{\mathrm{g}}$, and will be minimum otherwise, the value of $\kappa\delta$ is then given by

$$\kappa\delta = \left(2T_{\mathrm{g}} f_{\mathrm{min}} c + b\right) / \overline{F}_{\mathrm{R}}^{*}. \tag{14}$$

The actual average $\overline{F}_{\mathrm{R}}$ will be a little lower due to the made simplification. The amplitude of the continuous time signal $z(t)$ and the firing rate F_{R} at which the output samples are generated have a positive correlation. Thus the output time instances t_n occur closer together and further apart periodically with the same frequency f_{x} as the PRF of the spike train. The IF-TEM outputs nothing but the time instants t_n on which further DSP must be performed. As an heuristic approach on estimating the PRF f_{x} from the sequence of t_n, we evaluate the ML estimator, derived for the case of evenly spaced samples generated by a conventional ADC, using the time instants t_n instead. This is possible as the expression in (10) requires only samples of the periodic signal in the frequency domain that can be multiplied to the right of $\mathbf{C}$. Still, this near ML

This document is a preprint of: F. Roth, N. Bidoul, T. Rosca, *et al.*, "Spike-based sensing and communication for highly energy-efficient sensor edge nodes," in *Proc. 2nd IEEE Int. Hybrid Symp. Joint Communications & Sensing (JC&S)*, Accepted for publication, Innsbruck, Austria, Mar. 2022.

estimator is not ideal as it was designed for an AWGN channel and a receive filter such that it does not take into account the noise correlation introduced by additional integration. From the time instances t_n we generate the auxiliary signal

$$\bar{y}_n = \int_{t_{n-1}}^{t_n} z(t)\,\mathrm{d}t \Big/ (t_n - t_{n-1}) = \frac{\kappa\delta}{t_n - t_{n-1}} - b \quad (15)$$

assigned to the time instance t_{n-1}. Having a signal in time domain with non-evenly spaced samples, to retrieve a representation in the frequency domain the Lomb-Scargle periodogram is a well-known technique [22]. It gives an estimate of the PSD $S_{\bar{y}\bar{y}}(f_r)$ at arbitrary frequencies $f_r, r = 1, 2, \ldots, R$, which we write as vector $\mathbf{s} \in \mathbb{R}^{R\times 1}$. Using this representation of the periodic signal in the frequency domain, we estimate the PRF in a similar manner to (10) obtaining

$$\hat{f}_{\mathrm{x,TEM}} = \check{f}_{\mathrm{x},\hat{l}}, \quad \hat{l} = \underset{l}{\operatorname{argmax}}\ [\mathbf{C}'\,\mathbf{s}]_l, \quad (16)$$

where the elements of $\mathbf{C}' \in \mathbb{R}^{L\times R}$ are given by

$$[\mathbf{C}']_{l,r} = \left| \sum_{k=0}^{K-1} e^{j2\pi f_r \left(\frac{k}{\check{f}_{\mathrm{x},l}} + T_{\mathrm{g}}\right)} \right|^2. \quad (17)$$

V. Results

To evaluate the performance of our proposed sensory system, the entire processing chain was taken into account. Using the model of the VO_2 based oscillating circuit, the output signal $w(t)$ of the sensor could be generated for arbitrary input voltages yielding different oscillating frequencies f_{x}. This is followed by the simulated analog processing of $w(t)$ resulting in the spike train $x(t)$ including artefacts like the amplitude variations. Last, the wireless transmission and the estimation of the PRF at the receiver was simulated. When comparing both A/D conversion methods and their corresponding estimators, the bias of the IF-TEM was set heuristically to $b = 1.7\,c$ and $\kappa\delta$ was determined by (14) with $\overline{F}^*_{\mathrm{R}}$ being equal to the sampling rate $f_{\mathrm{s}} = 750\,\mathrm{kHz} > 2B_{\mathrm{g}}$ of the ADC. While the PSD of the IF-TEM output is computed for $R = 3000$ frequencies, the number of samples and frequencies generated by the ADC and DFT respectively is $N = Kf_{\mathrm{s}}/f_{\mathrm{min}}$. Furthermore both estimators check for $L = 3000$ values $\check{f}_{\mathrm{x},l}$, and in Fig. 5 and Fig. 6 there is no timing offset, i.e. $\Delta t = 0\,\mathrm{s}$. The performance of the estimators was evaluated in terms of the root mean squared error

$$\mathrm{RMSE} = \sqrt{\frac{1}{S}\sum_{s=1}^{S}(f_{\mathrm{x}}^{(s)} - \hat{f}_{\mathrm{x}}^{(s)})^2}. \quad (18)$$

In Fig. 5 and Fig. 7, $S = 1000$ signals of randomly chosen frequencies $f_{\mathrm{x}}^{(s)}$ were generated while in Fig. 6, $S = 500$. The RMSE is plotted in Fig. 5 over the signal-to-noise ratio (SNR) for $K = 20$ spikes along with its 95% confidence interval (CI) determined by bootstrapping. When computing the SNR, the signal and noise power is taken into account up to the point in time $t = K/f_{\mathrm{min}}$, regardless of the actual PRF. While the ML estimator using the evenly-spaced samples is more

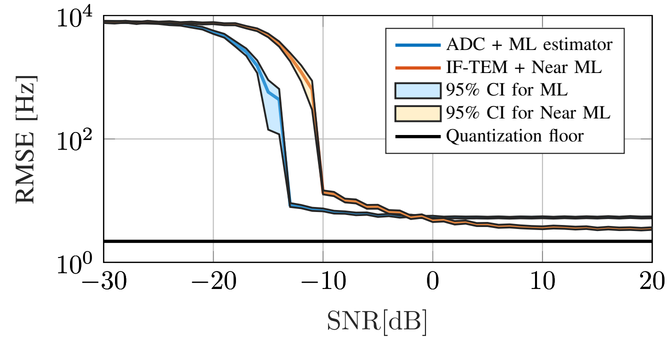

Fig. 5. RMSE of the estimate of the PRF f_{x} and its confidence interval over the SNR for $K = 20$ spikes.

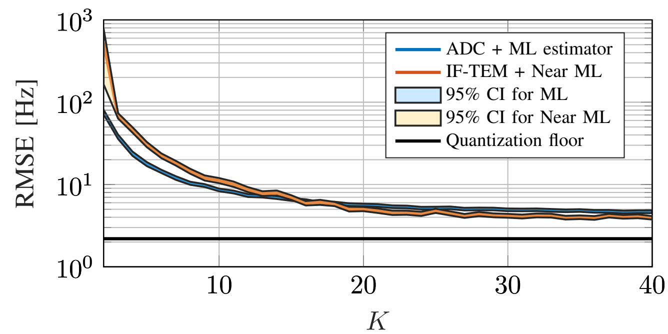

Fig. 6. RMSE of the estimate of the PRF f_{x} and its confidence interval over the number of pulses K at an SNR of $0\,\mathrm{dB}$.

robust to noise and performs reasonably well above an SNR of $-12\,\mathrm{dB}$, it is outperformed at an $\mathrm{SNR} \geq 0\,\mathrm{dB}$ by the heuristic estimator based on the IF-TEM output. The latter can profit from the unevenly-spaced samples allowing for a higher frequency resolution than the evenly-spaced samples provided by the ADC. Contrariwise, expression (16) was derived from the ML estimator for the AWGN channel. Possibly not considering the noise correlation introduced by the integration leads to a worse performance at low SNR. Additionally to the RMSE of the estimators, the minimum possible RMSE due to the discretization of $\check{f}_{\mathrm{x}}$ yielding $\check{f}_{\mathrm{x},l}$ is shown in the figures of this section. Among various distributions for $\check{f}_{\mathrm{x},l}$, the best results in terms of the RMSE were obtained for a logarithmic distribution which is used in the displayed figures, as the estimators are less robust against the deviation between the closest tested PRF $\check{f}_{\mathrm{x},l^*}$ and the true PRF f_{x} at smaller frequencies.

In Fig. 6 the RMSE is plotted over the number of pulses K at an SNR of $0\,\mathrm{dB}$. With its help it is possible to make a reasonable choice for K as, e.g., for $0\,\mathrm{dB}$ the estimation performance does not improve considerably above $K = 30$. It does not get worse either but in general we favor a shorter pulse train over a longer one as this way (i) the assumption of a slowly changing physical process and thus a constant PRF f_{x} is valid, (ii) computation time and (iii) computation complexity decreases at the receiver.

In Fig. 7 the RMSE is plotted over the timing offset Δt showing a substantial performance loss for the conventional ADC with ML estimator given only a small timing offset. On the other hand, the IF-TEM with the near ML estimator does not suffer from a positive timing shift up to $\Delta t = 850\,\mu\mathrm{s}$ and suffers only

This document is a preprint of: F. Roth, N. Bidoul, T. Rosca, *et al.*, "Spike-based sensing and communication for highly energy-efficient sensor edge nodes," in *Proc. 2nd IEEE Int. Hybrid Symp. Joint Communications & Sensing (JC&S)*, Accepted for publication, Innsbruck, Austria, Mar. 2022.

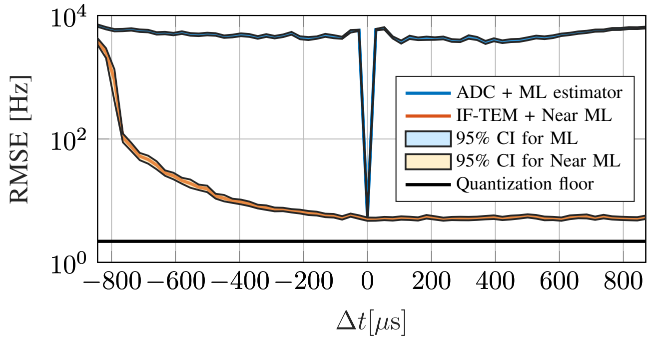

Fig. 7. RMSE of the estimate of the PRF f_x and its confidence interval over the timing shift Δt. $K = 20$ spikes are transmitted at an SNR of $0\,\mathrm{dB}$.

slowly from a negative shift down to the point where the short spike trains of high PRF are completely missed. However this different performance is not due to the different A/D conversion methods but mainly to the different estimators. While the ML estimator in (10), which was derived for $\Delta t = 0$, takes into account the phase of the spectrum, its adaption in (16) cannot do that as it operates on the PSD providing no phase information. In case of a timing shift which corresponds to a phase shift in frequency domain this is an advantage for the latter as it does not require accurate timing synchronization but it is sufficient if the receiver knows the start of the pulse train approximately. This could be realized by transmitting either every new pulse train on a predefined grid or a wake-up signal beforehand. The near ML estimator can also be used together with an ADC.

VI. Conclusion

In this work, we presented a first attempt for an all-spiking sensory system that operates in the analog domain up to the base station. Such a sensory system can work in combination with most conventional sensors, promises to lead to high energy efficiency by avoiding the conversion into the digital domain, and could be extended to perform joint communication and sensing using the emitted spike trains. We simulated the entire processing chain including an experimentally validated model of the VO_2-based VCO, a simple analog spike-generating circuit, the wireless channel, and the A/D conversion and estimation of the spike rate at the receiver. The performance of the proposed design was evaluated showing that the heuristic estimator for the spike rate using the samples of the IF-TEM outperforms the ML estimator for evenly-spaced samples at an $\mathrm{SNR} \geq 0\,\mathrm{dB}$. To improve the performance in the low SNR regime, the derivation of an estimator taking the noise correlation after integration into account is left open for future work. Further research is also required to incorporate amplitude and phase jitter introduced by the oscillator. Another interesting possibility includes leveraging the sensing functionality directly from the VO_2 device itself, which would enable event detection.

References

[1] C. MacGillivray and D. Reinsel, "Worldwide global DataSphere IoT device and data forecast, 2019-2023," ICD #US45066919, May 2019.

[2] A. S. G. Andrae and T. Edler, "On global electricity usage of communication technology: Trends to 2030," *Challenges*, vol. 6, no. 1, pp. 117–157, Jun. 2015.

[3] H. Malik, M. M. Alam, Y. L. Moullec, and A. Kuusik, "NarrowBand-IoT performance analysis for healthcare applications," *Procedia Computer Science*, vol. 130, pp. 1077–1083, Jan. 2018.

[4] W. Yi, K. K. Tsang, S. K. Lam, X. Bai, J. A. Crowell, and E. A. Flores, "Biological plausibility and stochasticity in scalable VO 2 active memristor neurons," *Nature Communications*, vol. 9, no. 1, p. 4661, Nov. 7, 2018.

[5] R. Lestienne, "Spike timing, synchronization and information processing on the sensory side of the central nervous system," *Progress in Neurobiology*, vol. 65, no. 6, pp. 545–591, Dec. 1, 2001.

[6] T. Rosca, F. Qaderi, M. Riccardi, O. J. Martin, and A. M. Ionescu, "An experimental study of the photoresponse of 1T-1R oscillators based on vanadium dioxide: Towards spiking sensing systems," in *Proc. of 21st International Conference on Solid-State Sensors, Actuators and Microsystems (Transducers)*, Jun. 2021, pp. 373–376.

[7] T. Birkoben, H. Winterfeld, S. Fichtner, A. Petraru, and H. Kohlstedt, "A spiking and adapting tactile sensor for neuromorphic applications," *Scientific Reports*, vol. 10, no. 1, p. 17 260, Oct. 14, 2020.

[8] K. Roy, A. Jaiswal, and P. Panda, "Towards spike-based machine intelligence with neuromorphic computing," *Nature*, vol. 575, no. 7784, pp. 607–617, Nov. 2019.

[9] G. de Streel, F. Stas, T. Gurné, F. Durant, C. Frenkel, A. Cathelin, and D. Bol, "SleepTalker: A ULV 802.15.4a IR-UWB transmitter SoC in 28-nm FDSOI achieving 14 pJ/b at 27 Mb/s with channel selection based on adaptive FBB and digitally programmable pulse shaping," *IEEE J. Solid-State Circuits*, vol. 52, no. 4, pp. 1163–1177, Apr. 2017.

[10] F. Roth, M. Dörpinghaus, and G. Fettweis, "Rate analysis of a spike-based signaling scheme for energy-efficient low rate communications," in *Proc. of 1st IEEE International Online Symposium on Joint Communications & Sensing (JC&S)*, Feb. 2021, pp. 1–6.

[11] C. Gimeno, D. Flandre, and D. Bol, "Analysis and specification of an IR-UWB transceiver for high-speed chip-to-chip communication in a server chassis," *IEEE Trans. Circuits Syst. I, Reg. Papers*, vol. 65, no. 6, pp. 2015–2023, Jun. 2018.

[12] G. Fettweis, M. Dörpinghaus, S. Bender, L. Landau, P. Neuhaus, and M. Schlüter, "Zero crossing modulation for communication with temporally oversampled 1-bit quantization," in *Proc. 53rd Asilomar Conf. Signals, Systems, and Computers*, Pacific Grove, CA, USA, Nov. 2019, pp. 207–214.

[13] P. Neuhaus, M. Schlüter, C. Jans, M. Dörpinghaus, and G. Fettweis, "Enabling energy-efficient Tbit/s communications by 1-bit quantization and oversampling," in *Proc. 2021 Joint European Conf. on Networks and Communications 6G Summit (EuCNC/6G Summit)*, Jun. 2021, pp. 84–89.

[14] B. Rumberg, D. W. Graham, V. Kulathumani, and R. Fernandez, "Hibernets: Energy-efficient sensor networks using analog signal processing," *IEEE J. Emerg. Sel. Topics Circuits Syst.*, vol. 1, no. 3, pp. 321–334, Sep. 2011.

[15] V. Sadhu, X. Zhao, and D. Pompili, "Energy-efficient analog sensing for large-scale and high-density persistent wireless monitoring," *IEEE Internet of Things Journal*, vol. 7, no. 8, pp. 6778–6786, Aug. 2020.

[16] X. Liang, H. Zhang, G. Fang, S. Ye, and T. A. Gulliver, "An improved algorithm for through-wall target detection using ultra-wideband impulse radar," *IEEE Access*, vol. 5, pp. 22 101–22 118, 2017.

[17] J. Lin, S. Ramanathan, and S. Guha, "Electrically driven insulator–metal transition-based devices—part i: The electrothermal model and experimental analysis for the dc characteristics," *IEEE Trans. Electron Devices*, vol. 65, no. 9, pp. 3982–3988, 2018.

[18] T. Rosca, F. Qaderi, and A. M. Ionescu, "High tuning range spiking 1R-1T VO2 voltage-controlled oscillator for integrated RF and optical sensing," in *Proc. 47th European Solid State Circuits Conf.*, Sep. 2021, pp. 183–186.

[19] B. Murmann. (2021). "ADC performance survey 1997-2021," [Online]. Available: http://web.stanford.edu/~murmann/adcsurvey.html.

[20] H. Naaman, S. Mulleti, and Y. C. Eldar, "FRI-TEM: Time encoding sampling of finite-rate-of-innovation signals," *arXiv:2106.05564*, Jun. 2021.

[21] A. Lazar and L. Toth, "Perfect recovery and sensitivity analysis of time encoded bandlimited signals," *IEEE Trans. Circuits Syst. I, Reg. Papers*, vol. 51, no. 10, pp. 2060–2073, Oct. 2004.

[22] N. R. Lomb, "Least-squares frequency analysis of unequally spaced data," *Astrophysics and Space Science*, vol. 39, no. 2, pp. 447–462, Feb. 1, 1976.